Correlation of β-Amyloid Aggregate Size and Hydrophobicity with Decreased Bilayer Fluidity of Model Membranes†

John J. Kremer, Monica M. Pallitto, Daniel J. Sklansky, and Regina M. Murphy*

Department of Chemical Engineering, University of Wisconsin—Madison, Madison, Wisconsin 53706-1607

Received February 1, 2000; Revised Manuscript Received May 24, 2000

ABSTRACT: β-amyloid peptide (Aβ) is the primary constituent of senile plaques, a defining feature of Alzheimer's disease. Aggregated Aβ is toxic to neurons, but the mechanism of toxicity remains unproven. One proposal is that Aβ toxicity results from relatively nonspecific Aβ−membrane interactions. We hypothesized that Aβ perturbs membrane structure as a function of the aggregation state of Aβ. Toward exploring this hypothesis, Aβ aggregate size and hydrophobicity were characterized using dynamic and static light scattering and 1,1-bis(4-anilino)naphthalene-5,5-disulfonic acid (bis-ANS) fluorescence. The effect of Aβ aggregation state on the membrane fluidity of unilamellar liposomes was assessed by monitoring the anisotropy of the membrane-embedded fluorescent dye, 1,6-diphenyl-1,3,5-hexatriene (DPH). Unaggregated Aβ at pH 7 did not bind bis-ANS and had little to no effect on membrane fluidity. More significantly, Aβ aggregated at pH 6 or 7 decreased membrane fluidity in a time- and dose-dependent manner. Aggregation rate and surface hydrophobicity were considerably greater for Aβ aggregated at pH 6 than at neutral pH and were strongly correlated with the extent of decrease in membrane fluidity. Prolonged (7 days) Aβ aggregation resulted in a return to near-baseline levels in both bis-ANS fluorescence and DPH anisotropy at pH 7 but not at pH 6. The addition of gangliosides to the liposomes significantly increased the DPH anisotropy response. Hence, self-association of Aβ monomers into aggregates exposes hydrophobic sites and induces a decrease in membrane fluidity. Aβ aggregate-induced changes in membrane physical properties may have deleterious consequences on cellular functioning.

β-amyloid (Aβ)[1] is a 39−43 amino acid peptide derived from proteolytic cleavage of the large membrane-anchored amyloid precursor protein (APP). Aβ aggregates into fibrils that constitute the principal proteinaceous ingredient of cerebrovascular amyloid deposits and senile plaques, two of the distinctive pathological features of Alzheimer's disease (AD). In vitro, toxicity of Aβ is clearly correlated with aggregation into cross-β-pleated sheet fibrils (*1*, *2*). The exact mechanism of Aβ neurotoxicity is debated; for review, see Iverson et al. (*3*) or Mattson (*4*). Several groups have proposed that Aβ associates specifically with cells via membrane-bound receptors (*5*−*9*). However, the discoveries that both D- and L-enantiomers of Aβ produce fibrillar aggregates with identical structural and cytotoxic properties (*10*) and that fibrils consisting of either amylin or Aβ, with similar structure but distinct sequence, induce similar changes in gene expression (*11*) suggest that the interaction between Aβ and neurons may not be mediated via specific Aβ−receptor association.

An alternative hypothesis is that Aβ aggregates are toxic via nonspecific association with cell membranes. There is growing evidence indicating that Aβ−membrane interactions occur that affect both peptide and membrane properties. For example, Aβ binds to rat cortical homogenates in vitro in an aggregation-dependent manner (*12*). Membrane components promoted changes in Aβ secondary structure and/or aggregation propensity (*13*−*17*). Aβ or its fragments reportedly cause the formation of large ion channels in phospholipid planar bilayers (*18*), leakage of encapsulated dyes from phospholipid vesicles (*17*, *19*), fusion of small unilamellar vesicles (*20*), imposition of negative curvature strain on ganglioside-containing lipid bilayers (*21*), and loss of impermeability in lysosomal and endosomal membranes (*22*). Together these data suggest that Aβ associates with membranes and alters normal membrane properties. This association may have adverse consequences for cellular viability, since compounds that inhibited Aβ association with membranes also prevented Aβ toxicity in vitro (*23*).

One important structural feature of membranes is the fluidity of the bilayer, because of its influence on proper functioning of membrane-bound proteins. A few inconsistent results have emerged regarding the effect of Aβ on membrane fluidity. Müller et al. (*24*, *25*) observed decreases in

† Funding was provided by grants from the National Institute of Aging (AG14079), the Alzheimer's Association (RG1-96-012), an SC Johnson Distinguished Fellowship, and NIH Chemistry-Biology Interface Training Grant 5 T32 GM08505 (J.J.K.).

* To whom correspondence should be addressed. Phone: (608) 262-1587. Fax: (608) 262-5434. E-mail: murphy@che.wisc.edu.

[1] Abbreviations: Aβ, β-amyloid peptide (1−39) or (1−40); AD, Alzheimer's disease; bis-ANS, 1,1-bis(4-anilino)naphthalene-5,5-disulfonic acid; APP, amyloid precursor protein; BHT, butylated hydroxy toluene; BSA, bovine serum albumin; Chol, cholesterol; DMSO, dimethyl sulfoxide; DPH, 1,6-diphenyl-1,3,5-hexatriene; FPLC, fast performance liquid chromatography; HPLC, high performance liquid chromatography; n-PG, *n*-propyl gallate; PBS, phosphate buffered saline, 10 mM KH_2PO_4/K_2HPO_4, 150 mM NaCl; POPC, 1-palmitoyl-2-oleoyl-sn-glycero-3-phosphocholine; POPE, 1-palmitoyl-2-oleoyl-sn-glycero-3-phosphoethanolamine; POPG, 1-palmitoyl-2-oleoyl-sn-glycero-3-[phospho-rac-(1-glycerol)]; POPS, 1-palmitoyl-2-oleoyl-sn-glycero-3-[phospho-l-serine]; ThT, thioflavin T.

10.1021/bi0001980 CCC: $19.00
Published on Web 07/21/2000

membrane fluidity when Aβ was added to mouse brain or human cortex membrane homogenates embedded with DPH. Sonication of Aβ with phospholipids and cardiolipin also induced a decrease in membrane fluidity (*26*). In contrast, when Aβ was mixed with rat synaptic plasma membrane constituents embedded with the fluorescent dye pyrene, increases in annular and bulk fluidity were observed (*27, 28*).

To further clarify the effect of Aβ on membrane fluidity, we measured changes in DPH anisotropy in a model membrane system. Specifically, we tested the effect of Aβ on anisotropy of DPH embedded in large unilamellar vesicles of pure 1-palmitoyl-2-oleoyl phosphatidylcholine (POPC) and 1-palmitoyl-2-oleoyl phosphatidylglycerol (POPG), as well as in vesicles composed of mixtures of phospholipids, cholesterol, and gangliosides that more closely mimic neuronal membranes (*29*−*31*). DPH anisotropy has been used extensively to measure lipid order (*32*−*34*) and specifically reports on phospholipid acyl chain dynamics (*35*−*36*). Since aggregation is a requisite precondition for toxicity (*3*), we explored whether changes in membrane fluidity were correlated with Aβ aggregation state. The rate of growth of Aβ aggregates was monitored by dynamic and static light scattering. The fluorescent dye bis-ANS, frequently used in protein refolding studies, was used to quantify changes in exposure of hydrophobic sites on Aβ with aggregation and to correlate hydrophobic exposure to membrane response. Our intentions were (i) to compare our results to literature data regarding effects of Aβ on membrane fluidity, (ii) to determine whether any such effects observed with biological membranes could be attributed to specific membrane components, and (iii) to ascertain whether these changes depended on the aggregation state of Aβ. This latter point is of particular interest because we believe that any plausible mechanism of neurotoxicity must account for the observations that aggregated but not monomeric Aβ is toxic.

EXPERIMENTAL PROCEDURES

Materials. Synthetic Aβ peptides were purchased from AnaSpec Inc. (San Jose, CA). Purity was >95% by HPLC; correct molecular mass was confirmed by mass spectroscopy. Lyophilized Aβ peptides were stored at −70 °C until use. Cleavage of APP generates Aβ fragments of variable length (39−43 amino acids), with Aβ(1−40) the most common fragment in biological samples (*37*). For work reported here, the more soluble shorter fragments, Aβ(1−39) and Aβ(1−40), were used. Data in Figures 1−5 and 9 and in Tables 1 and 3 were collected using Aβ(1−40), while data reported in Figures 7 and 8 and in Table 2 were collected using Aβ-(1−39). Several DPH anisotropy experiments were run using both Aβ(1−39) and Aβ(1−40); no significant differences were observed (data not shown).

POPG, POPC, 1-palmitoyl-2-oleoyl-sn-glycero-3-phosphoethanolamine (POPE), 1-palmitoyl-2-oleoyl-sn-glycero-3-[phospho-l-serine] (POPS), and cholesterol (Chol) were purchased from Avanti Polar Lipids (Alabaster, AL). Mixed gangliosides, poly-L-lysine (molecular mass: 4−15 and 500 kDa), bovine serum albumin (BSA), diphenylhexatriene (DPH), *n*-propyl gallate (n-PG), and HPLC (99.9%)-grade dimethyl sulfoxide (DMSO) were purchased from Sigma Chemical Co. (St. Louis, MO). Bis-ANS was purchased from Molecular Probes (Eugene, OR). Phospholipids were stored in chloroform at −20 °C. Cholesterol and gangliosides were stored as solids at −20 °C.

Aβ Sample Preparation. Excess water was removed from DMSO using molecular sieves (Sigma). Lyophilized Aβ was dissolved in DMSO at 10 mg/mL for at least 60 min. This treatment disrupts β-sheet secondary structure (*38*) and renders Aβ apparently monomeric as measured by analytical ultracentifugation (unpublished data) and as reported by others (*39*). Aβ stock solution was diluted 20-fold in phosphate-buffered saline (PBS: 10 mM KH_2PO_4/K_2HPO_4 and 150 mM NaCl, pH 6 or 7) to a final concentration of 0.5 mg/mL (∼115 μM equivalent monomer concentration) and allowed to aggregate at room temperature for 1−7 days (*38*). Freshly prepared samples were either diluted in the same fashion and used immediately or kept in pure DMSO (at 10 mg/mL) until direct dilution into the fluorescence cuvette.

Light Scattering. Static and dynamic light scattering were used to characterize the rate of growth and the size of Aβ aggregates. Samples were prepared as described above, except PBSA (PBS with 0.02% sodium azide, pH 6 or 7.4) was double-filtered through 0.22-μm filters prior to use. Samples were briefly vortexed, quickly transferred into clean light-scattering cuvettes, and placed in a temperature-controlled (25 °C) bath of decahydronaphthalene. Dynamic light scattering data was collected using a Lexel (Fremont, CA) argon laser and a Malvern (Southborough, MA) 4700C system as described in more detail elsewhere (*40*). Briefly, autocorrelation functions were measured at 90° scattering angle over several days. Data were fit using the method of cumulants to derive a *z*-averaged translational diffusion coefficient and then converted to an average apparent hydrodynamic diameter of an equivalent sphere, d_{sph}. Static light-scattering measurements were taken at several time points with the same samples and apparatus, as described in more detail elsewhere (*41*). Data were plotted in the Kratky format, $q^2R_s(q)/Kc$ [$= q^2<M>_wP(q)$] vs q, where q is the scattering vector and is a function of the scattering angle, $R_s(q)$ is the Rayleigh ratio calculated from the scattered light intensity measurements, K is an instrument constant, c is the peptide mass concentration, $<M>_w$ is the weight-averaged molecular weight, and $P(q)$ is the particle scattering factor, which is a function of particle shape and dimension. Second virial coefficient corrections were ignored. Data were fit using a semiflexible chain model for the particle shape to determine $<M>_w$, the total length of the fibril L_c, and the Kuhn statistical segment length l_k, a measure of fibril stiffness (*41*). Alternatively, the semiflexible star model was used to determine $<M>_w$, L_c, l_k, and f_b, the number of branches (*41*). Data were fit using the nonlinear regression analysis program GREG (*42*).

Electron Microscopy. Aβ solutions were prepared at pH 6 and 7 as described above and then aggregated for 2 days. The samples were vortexed for 10 s, then 12 μL of the peptide solution was mixed with one drop of 2% ammonium molybdate and placed on a freshly prepared Pioloform-coated Cu 400-mesh grid (Electron Microscopy Sciences, Fort Washington, PA) for 1 min. The excess was blotted, and the grid was allowed to dry. The prepared samples were imaged on a Philips (Briarcliff Manor, NY) CM120 Scanning Transmission Electron Microscope at 80 kV.

Size Exclusion Chromatography. The relative distribution of monomer, oligomer, and large aggregates was measured with size exclusion chromatography. A Superdex 75 PC 3.2/30 precision size-exclusion column plumbed to an FPLC system (Pharmacia, Piscataway, NJ) was calibrated with PBSA, pH 7.4, as the mobile phase, with the following proteins as molecular mass standards: insulin chain B (3.5 kDa), ubiquitin (8.5 kDa), ribonuclease A (13.7 kDa), ovalbumin (43 kDa), and BSA (67 kDa). The column's exclusion limit for globular proteins is 100 kDa. Small aliquots of Aβ samples prepared for light-scattering experiments were injected into the column. The apparent molecular weight was determined by comparison to calibration data.

Bis-ANS Fluorescence. Fluorescence of the dye bis-ANS was used to measure the relative exposure of hydrophobic surfaces on Aβ aggregates (*43*, *44*). Bis-ANS was dissolved in PBS, pH 7, to a concentration of 20 μM. Fluorescence intensity measurements were taken using a PTI (South Brunswick, NJ) spectrofluorometer, with the excitation wavelength at 360 nm and the emission spectra read from 450 to 550 nm. Baseline measurements of bis-ANS in buffer were taken first, and then Aβ was added to the fluorescence cuvette to a final concentration of 2 μM. Increasing the Aβ concentration increased bis-ANS fluorescence, whereas decreasing the bis-ANS concentration to 10 μM did not decrease the fluorescence signal (data not shown), demonstrating that these experiments were run under excess dye conditions. DMSO and PBS had no effect on bis-ANS fluorescence (data not shown).

Liposome Preparation. Unilamellar single-component (POPC or POPG) and multicomponent vesicles were prepared by extrusion. Type 1 and 2 vesicles consist of POPC/POPE/POPS/Chol (36:36:10:18) and POPC/POPE/POPS/Chol/gangliosides (33:33:10:16:8) by mass percent, respectively. Cholesterol and gangliosides were dissolved in chloroform or methanol and mixed with phospholipids stored in chloroform. DPH was dissolved in chloroform and added to the phospholipid solutions at a 1:500 (DPH/phospholipid) molar ratio to ensure incorporation of DPH into the vesicles. DPH/phospholipid solutions were dried under N_2 gas followed by 1 h of vacuum desiccation and overnight storage in a desiccated container. Samples were stored at −20 °C. Dried samples were dissolved in PBS pH 7 at 5 mg/mL, allowed to equilibrate for 30 min, and then passed at least 20 times through an extruder (Avanti Polar Lipids) with a 100-nm membrane pore size. Exposure to light was minimized throughout the liposome preparation process. Liposome diameter was verified at ∼125 nm (polydispersity ∼0.14) by dynamic light scattering.

Membrane Fluidity Measurements. Anisotropy measurements were obtained using a PTI spectrofluorometer equipped with manual polarizers. Excitation and emission wavelengths were set at 360 and 430 nm, respectively. The *g*-factor was measured as described and used in the anisotropy calculation as shown in eq 1 (*45*). Liposomes with embedded DPH were diluted to 250 μM (phospholipid concentration) with PBS. Aliquots of Aβ solutions were titrated into the liposome-containing buffer and equilibrated for 10−20 min after each addition. Preliminary results indicated this was sufficient time to reach steady-state (data not shown). The pH of the Aβ and liposome solutions were matched such that Aβ incubated at pH 6 was added to vesicles at pH 6 and likewise for pH 7. For each sample, fluorescence emission intensity data in parallel and perpendicular orientations were collected four times each and then averaged. No more than 4−5 anisotropy measurements were taken on a given sample to prevent DPH bleaching artifacts. For a given liposome sample, total fluorescence intensity generally decreased <10% due to dilution and photobleaching combined. All measurements were at room temperature. Anisotropy *r* was calculated as:

$$r = \frac{I_{par} - gI_{per}}{I_{par} + 2gI_{per}} \quad (1)$$

where I_{par} = parallel intensity, I_{per} = perpendicular intensity, and g = *g*-factor. For a completely rigid immobile molecule, $I_{par} = 3I_{per}$ and $r = 0.4$ (*45*). The maximum observable DPH anisotropy in membranes is limited to 0.3−0.34 (*35*). Anisotropy was plotted versus Aβ concentration, and the slope and intercept were determined by linear regression fits using Microsoft Excel.

As controls, poly-L-lysine or BSA were dissolved in a 5% DMSO/PBS (pH 6 or 7) solution at 5 mg/mL (for 4−15 kDa poly-lysine), 10 mg/mL (for 500 kDa poly-lysine), and 0.5 mg/mL (for BSA) and then diluted into liposome solutions and analyzed as described above.

Lipid Peroxidation. To ascertain whether Aβ induced lipid peroxidation, the method of Walter et al. (*46*) was used with minor modifications. Briefly, Aβ(1−40) was aggregated for 2 days at 115 μM (0.5 mg/mL) at pH 6 or 7 and added to vesicles (1 mg/mL) to a final Aβ concentration of 11.5 μM. A 100 μL aliquot was added to 1 mL of CHOD-iodide reagent (*47*), 20 μL of BHT in ethanol (35 mM), and 80 μL of sodium azide (5 mM) for 3 h, centrifuged (∼15000*g*), and filtered at 0.2 μm to eliminate turbidity effects, and absorbance was measured at 365 nm. Alternatively, DPH anisotropy experiments were carried out in the presence of the antioxidant, n-PG.

RESULTS

Characterization of Aβ Aggregate Size, Growth Kinetics, and Morphology. Monomeric Aβ spontaneously converts to fibrillar aggregates at physiologically relevant conditions. Size-exclusion chromatography and laser light-scattering were used to characterize Aβ aggregate size and distribution as a function of pH and time. On a calibrated Superdex column, freshly diluted Aβ at neutral pH eluted as two overlapping peaks with residence times corresponding to Aβ monomers and dimers (data not shown). Freshly diluted Aβ at pH 6 produced a single broad peak, with a significantly smaller area, that eluted with a retention time corresponding to a mixture of monomer−dimer species. Peaks at the void (100 kDa for globular proteins), but no intermediate species, were detected at pH 6. By comparing monomer/dimer peak areas with calibration curves, we estimated that ∼75% of Aβ at pH 7, but only ∼20% of Aβ at pH 6, was monomer/dimer, with the remainder present as aggregates. To provide another measure of the fraction of peptide in aggregated form, Aβ samples were prepared at pH 6 or 7, incubated for 2 days, and then centrifuged for 5 min at 12000*g*. These conditions are sufficient to pellet much, but not all, aggregated Aβ. The percent of Aβ in the supernatant phase was ∼67% at pH 7 and ∼15% at pH 6 using a Lowry assay (Sigma).

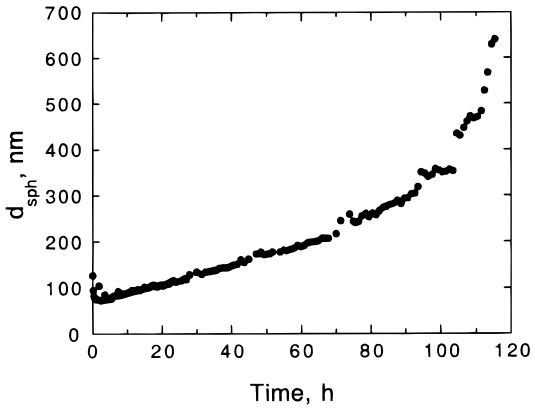

FIGURE 1: Growth kinetics of Aβ aggregates at physiological pH. Aβ was dissolved in DMSO and then diluted 20-fold into PBS, pH 7.4, to a final concentration of 0.5 mg/mL. The average apparent hydrodynamic diameter, d_{sph}, was determined from cumulants analysis of dynamic light-scattering data taken at 90° scattering angle.

Immediately upon dilution of Aβ from DMSO stock solution into PBS at pH 6, the sample become optically turbid, indicative of formation of macroscopic aggregates. This rapid precipitation precluded collection of light-scattering data. In contrast, Aβ samples diluted into PBSA at physiological pH remained optically clear for several days. The rate of growth of Aβ aggregates was characterized by dynamic light scattering (Figure 1). Large aggregates were present within minutes of dilution, with an initial hydrodynamic diameter d_{sph} of ~75 nm. Assuming a rigid-rod morphology, this corresponds to a fibril length of ~300 nm (*48*). The average d_{sph} increased linearly with time for ~90 h (4 days). Between 90 and 110 h, fibril growth rate was accelerated until the appearance of macroscopic aggregates that precipitated at ~110 h (5 days).

Additional detailed information on Aβ growth kinetics, aggregate size, and morphology was obtained by collecting static light-scattering data on the same samples. Data are presented in the Kratky format (Figure 2). The shapes of the curves at times up to 52 h are characteristic of a semiflexible fibril morphology (*38*). At longer times (69 and 93 h), a maximum at intermediate values of q is indicative of the onset of a branched structure, which we attribute to fibril−fibril entanglement as fibrils become sufficiently long. The data were fit to model equations for $P(q)$ of semiflexible chains (24−52 h) or semiflexible stars (69−93 h), as shown in Figure 2. Size parameters were extracted from these fits and are summarized in Table 1. Both average molecular weight $<M>_w$ and average fibril length L_c increased linearly over the first 4 days (Figure 3). The ratio $<M>_w/L_c$ was constant with time, indicating that the increase in average aggregate size is due predominantly to fibril elongation rather than new fibril formation. A modest level of fibril entanglement (number of branches = 3−4) at longer times was detected. The onset of visible precipitates at ~110 h precluded further data collection.

Aβ samples were prepared at pH 6 or pH 7, incubated at room temperature for 2 days, and then observed under an electron microscope. Distinct differences in morphological features of Aβ aggregates prepared at neutral vs acidic pH were apparent (Figure 4). Specifically, long semiflexible fibrils of ~10 nm diameter were present in the pH 7 sample

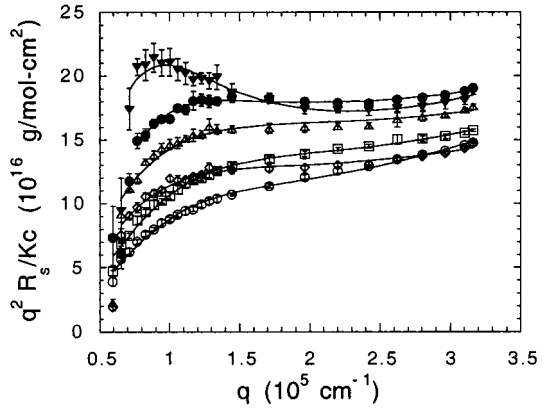

FIGURE 2: Change in Aβ aggregate molecular weight and size with time. Aβ was dissolved in DMSO and then diluted 20-fold into PBSA, pH 7.4, to a final concentration of 0.5 mg/mL. Static light-scattering data taken at 24 (○), 30 (□), 44 (◇), 52 (△), 69 (●), and 93 h (▼) after initiation of aggregation are shown as Kratky plots. Lines indicate nonlinear regression fit of semiflexible chain (24−52 h) or semiflexible star (69−93 h) models to the data. The increase in the *y*-axis intercept is indicative of an increase in average molecular weight, whereas the appearance of a maximum in the curves at intermediate values of q is characteristic of branched structures. Molecular size parameters extracted from data fitting are listed in Table 1.

Table 1: Size Characteristics of Aβ Aggregates

time (h)	$<M>_w$[a] (10^6 Da)	L_c (nm)	l_k (nm)	f_b
24	18 ± 1	960 ± 5	200 ± 20	ND[b]
30	22 ± 2	1160 ± 60	160 ± 15	ND
44	34 ± 3	1960 ± 140	150 ± 20	ND
52	43 ± 4	2100 ± 180	140 ± 20	ND
69	49 ± 3	2800 ± 400	120 ± 20	3.0 ± 0.4
93	80 ± 10	4000 ± 800	140 ± 30	4.2 ± 0.8

[a] Average molecular weight $<M>_w$, average fibril length L_c, average Kuhn statistical length l_k, and average number of branches f_b were determined from nonlinear regression fit of data shown in Figure 2 to equations for semiflexible chain and star models. Error estimates represent 95% confidence intervals for fitted parameters. [b] ND = not determined.

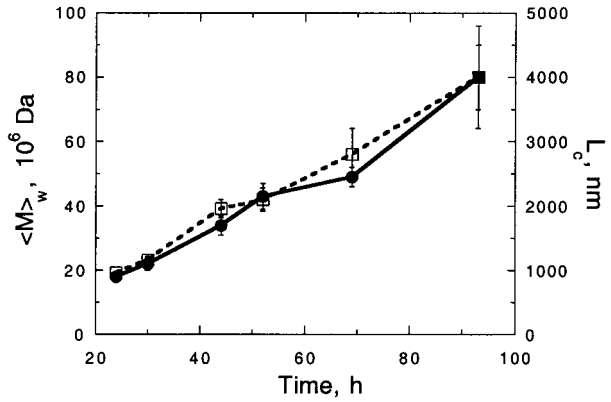

FIGURE 3: Growth of Aβ aggregates at physiological pH. Weight-averaged molecular weight $<M>_w$ (●) and average fibril length L_c (□) were determined by nonlinear regression fit of model equations to the light-scattering data of Figure 2, as described in more detail in the text. Error bars represent 95% confidence intervals for fitted parameters.

(Figure 4A), consistent with observations by light scattering. In contrast, amorphous aggregates were observed at pH 6 (Figure 4B). Despite these differences in gross morphology, both samples caused an increase in ThT fluorescence (data

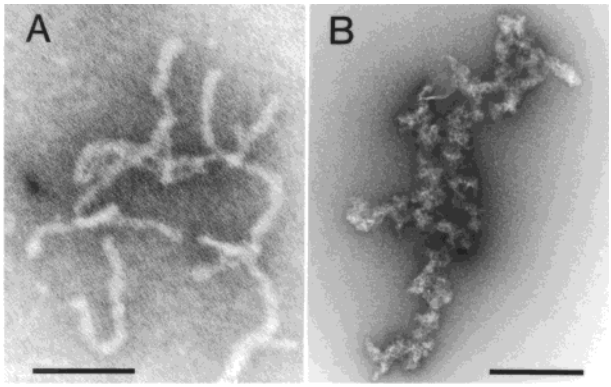

FIGURE 4: Electron micrographs of Aβ aggregated for 2 days at neutral and acidic pH. (A) pH 7 fibrillar aggregates, scale bar = 50 nm; (B) pH 6 agglomerated aggregates; scale bar = 200 nm.

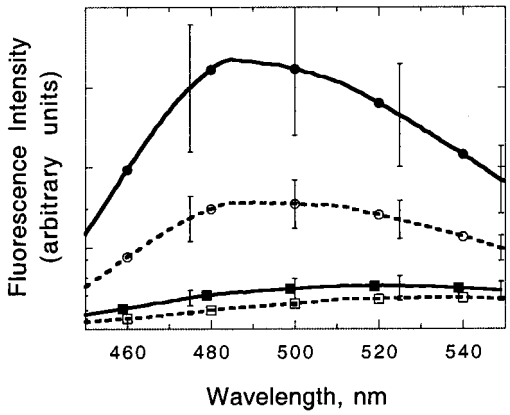

FIGURE 5: Effect of Aβ aggregation on bis-ANS fluorescence. PBS (□, $n = 18$), freshly diluted Aβ (■, $n = 4$), and Aβ aggregated for 2 days in PBS at pH 7 (○, $n = 6$) or pH 6 (●, $n = 6$) were added to PBS containing the dye bis-ANS. Fluorescence spectra were collected from 450 to 550 nm, with excitation at 360 nm. Results shown are averaged scans from 4−18 samples; the error bars signify one standard deviation. Two other data sets were taken with samples prepared on different days with similar results (data not shown). Binding of bis-ANS to exposed hydrophobic sites is signaled by an increase in fluorescence intensity and blue-shifting of the peak. Fluorescence intensity of Aβ aggregated at pH 6 and 7 was statistically different ($p < 0.01$).

not shown), a dye frequently used to detect extended cross-β-sheet structure characteristic of amyloid fibrils (*49*).

Surface Hydrophobicity of Aβ Aggregates. The fluorescent dye bis-ANS, which is widely used in protein refolding studies (*50*, *51*), was employed to gather additional information about the structural features of Aβ aggregates. Bis-ANS binds to solvent-exposed hydrophobic patches on protein surfaces, producing an increase in fluorescence intensity and blue-shifting of the emission maximum (*43*, *44*). Monomeric Aβ had no effect on bis-ANS fluorescence (Figure 5). Bis-ANS fluorescence intensity increased severalfold when mixed with Aβ aggregated for 2 days at pH 6 or 7, with the pH 6 sample having a significantly greater effect (Figure 5). Both spectra showed a blue-shift in the emission maximum to ∼485−495 nm, with pH 6 aggregates slightly more blue-shifted by ∼5−10 nm. A sample of Aβ aggregated at pH 7 for 2 days was centrifuged, the supernatant was removed, and the pellet was washed and resuspended. Both supernatant and resuspended pellet caused approximately equivalent increases in bis-ANS fluorescence intensity, when corrected for Aβ concentration (data not shown). This

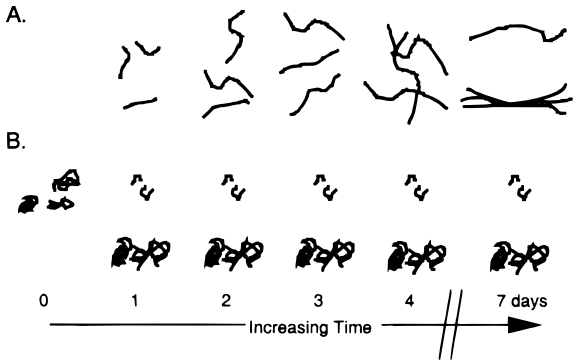

FIGURE 6: Sketch of Aβ aggregation at (A) neutral and (B) acidic pH. (A) At pH 7, Aβ steadily increases from an average fibril length of ∼960 nm at 1 day to ∼4000 nm at 4 days (Table 1). These fibrils possess hydrophobic patches as shown by bis-ANS binding (Figure 5). Fibril−fibril entanglement is detectable as "branching" at 3 days and increases with time (Table 1). Precipitation occurs around 5 days, accompanied by a loss of bis-ANS binding when tested at 7 days. Together these results suggest that at the later stages of Aβ aggregation at neutral pH, fibril−fibril association mediated by hydrophobic interaction occurs, reducing solvent-exposed hydrophobic patches but generating macroscopic fibril bundles. (B) At pH 6, Aβ instantaneously forms large, amorphous aggregates that precipitate in less than 24 h. These aggregates contain many highly hydrophobic solvent-exposed patches, which are present even at 7 days. This suggests that Aβ aggregation at pH 6 does not occur through orderly self-association via burial of hydrophobic interactions and that precipitation occurs due to poor aggregate solubility near the isolectric point.

indicates that soluble aggregates can bind bis-ANS. (The supernatant phase scattered light, indicating that some aggregates were still present in solution.) Surprisingly, if Aβ was aggregated for 7 days at pH 7, fluorescence intensity returned to near background levels (data not shown). In contrast, there was no decrease in bis-ANS fluorescence with prolonged (7 days) incubation of Aβ at pH 6.

Results from light scattering, electron microscopy, and bis-ANS fluorescence experiments are summarized schematically in Figure 6. Briefly, upon dilution of monomeric Aβ into PBS at pH 6, ∼80−85% of the peptide is rapidly converted to precipitable macroaggregates lacking a well-defined linear fibrillar structure and possessing considerable surface hydrophobicity. With dilution into PBS at pH 7, ∼25−35% of Aβ is converted to aggregates of fibrillar morphology that remain soluble and elongate steadily over the course of ∼4 days. Eventually (after 5 days), a second phase appears. The soluble fibrils contain surface hydrophobic patches, but this property disappears after prolonged (1 week) incubation.

Aβ-Induced Changes in Membrane Fluidity of Single-Component Liposomes. In POPG or POPC liposomes at pH 6 or 7, DPH anisotropy was ∼0.14. When freshly diluted Aβ at pH 7 was added to liposomes, there was no effect on DPH anisotropy with POPC liposomes and a modest effect with POPG liposomes (Figure 7). In contrast, when Aβ was aggregated at pH 7 for 2 days prior to addition to liposomes, there was a marked increase in DPH anisotropy that was linear with increasing Aβ concentration (Figure 7). This effect was somewhat greater with POPG as compared to POPC vesicles. Control solutions of BSA and poly-lysine, or dilution of liposomes with DMSO or additional PBS, had no effect on DPH anisotropy (data not shown). Somewhat different results were obtained at pH 6. Freshly prepared Aβ

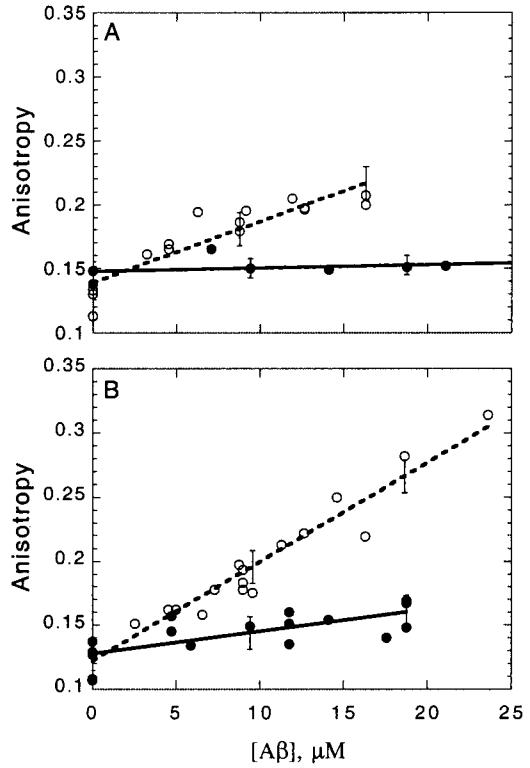

FIGURE 7: Effect of Aβ aggregation at pH 7 on DPH anisotropy. Aβ was dissolved in DMSO and then diluted 20-fold into PBS, pH 7. Freshly prepared (●) and 2 day-aged (○) Aβ solutions were titrated into (A) POPC or (B) POPG liposomes with embedded DPH. Fluorescence intensity measurements were taken in parallel and perpendicular orientations, and the anisotropy was calculated per eq 1. Data shown are a compilation of 2−4 replicate experiments at each condition. Lines are linear regression fits of the compiled data. Error bars are ±1 standard error of the fitted data.

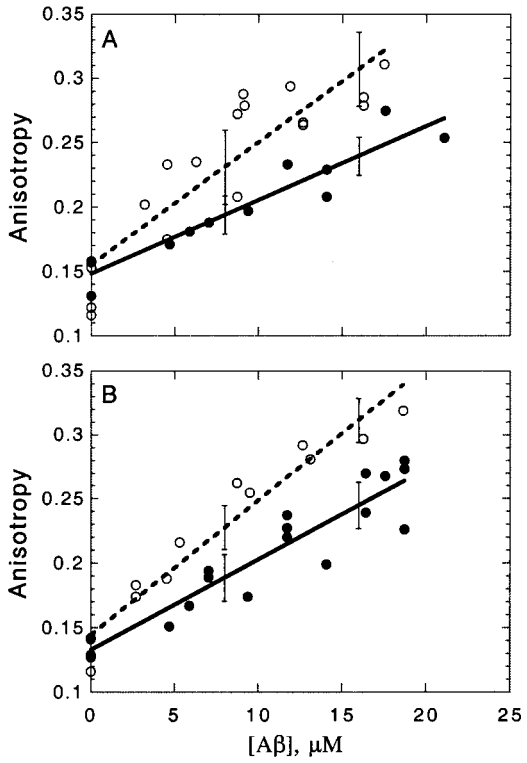

FIGURE 8: Effect of Aβ aggregation at pH 6 on DPH anisotropy. Aβ was dissolved in DMSO and then diluted 20-fold into PBS, pH 6. Freshly diluted (●) and 2 day-aged (○) Aβ samples were added to (A) POPC and (B) POPG liposomes with embedded DPH. Data shown are a compilation of 2−4 replicate experiments at each condition. Lines are linear regression fits of the compiled data.

at pH 6 caused a dose-dependent increase in DPH anisotropy for both POPG and POPC liposomes (Figure 8). This effect was rapid, since when Aβ in DMSO was diluted directly into a solution of liposomes at pH 6, the anisotropy reached steady-state at 10 min after dilution and was >80% of this steady-state value at 3 min after dilution, the earliest time point recorded (data not shown). When Aβ was aggregated for 2 days at pH 6, the increase in anisotropy was even more pronounced (Figure 8). Under some conditions, DPH anisotropy increased to values equal to that obtained for POPC below its gel transition temperature, where $r = 0.33$ (*52*).

To further explore the time-dependence of Aβ-induced changes in membrane fluidity, Aβ was aggregated for 1−4 days at pH 6 or 7, then tested in the DPH assay. Results are summarized in Table 2. At pH 7, DPH anisotropy increased over the first 2 days, with a greater increase from day 0 to day 1. Interestingly, there was a small but statistically significant decline in anisotropy at 4 days. At all time points, the change in DPH anisotropy was greater for POPG than for POPC liposomes. At pH 6, the change in DPH anisotropy with concentration increased from 0 to 2 days of aggregation and then plateaued. No change in anisotropy with longer (4 days) aging time was observed. There was a consistent, but not statistically significant, difference between POPC and POPG liposomes at pH 6. Taken together, the data indicate that Aβ induced decreases in membrane fluidity in an age- and pH-dependent manner. Qualitatively, these results mirror the age- and pH-dependent changes in Aβ physical properties: freshly diluted monomeric Aβ at pH 7 was unable to induce changes in bis-ANS fluorescence or DPH anisotropy; Aβ at pH 6 aggregated more rapidly and completely, caused a greater increase in bis-ANS fluorescence, and induced larger changes in DPH anisotropy than did Aβ at pH 7.

Table 2: Effect of Aggregation, pH, and Phospholipid Type on Aβ-Induced Changes in DPH Anisotropy[a]

	POPC		POPG	
	pH 7	pH 6	pH 7	pH 6
freshly prepared	0.3 ± 0.3	5.7 ± 0.6	1.7 ± 0.5	7.0 ± 0.6
1 day aged	3.4 ± 0.6	7 ± 1	6.1 ± 0.7	8.0 ± 0.4
2 days aged	5.4 ± 0.7	9 ± 1	7.7 ± 0.5	10.4 ± 0.8
3 days aged	4.9 ± 0.8	10.1 ± 0.6	7 ± 1	12 ± 1
4 days aged	3 ± 1	10 ± 1	4 ± 1	11.0 ± 0.9

[a] Aβ (0.5 mg/mL) was aggregated in PBS at pH 6 or pH 7 for the indicated length of time and then diluted into solutions of POPC or POPG liposomes containing embedded DPH. Anisotropies were calculated from measured fluorescence intensities in the parallel and perpendicular orientation and plotted vs Aβ concentration. Slopes (10^{-3} anisotropy units/μM of Aβ) and standard errors shown in the table were obtained from linear regression fit of anisotropy data plotted vs Aβ concentration.

Given the differences in time dependence for the pH 6 vs pH 7 samples, we next aged Aβ for 7 days and tested preparations in the DPH assay. At pH 6, the increase in DPH anisotropy at 2 and 7 days aggregation time was comparable. Surprisingly, at pH 7, the increase in DPH anisotropy after 7 days aggregation was reduced to about 20% of the value obtained after 2 days. These results correlate strongly with the bis-ANS fluorescence data: at pH 6, bis-ANS fluorescence was the same at 2 and 7 days, whereas at pH 7, bis-

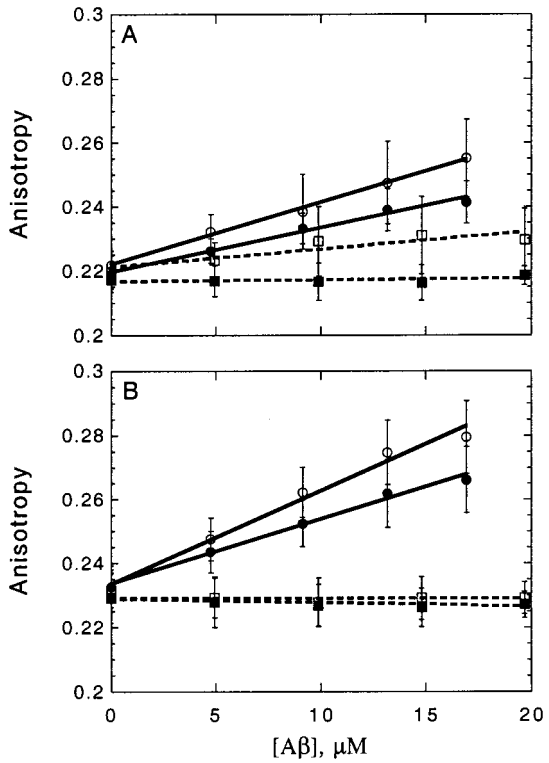

FIGURE 9: DPH anisotropy with (A) type 1 and (B) type 2 vesicles at pH 7 (−●−, - - -■- - -) and pH 6 (−○−, - - -□- - -) upon addition of freshly diluted (- - -■- - -, - - -□- - -) and 2 day-aged (−●−, −○−) Aβ. Measurements were taken as described in Figures 7 and 8. Aged Aβ induces a significantly larger anisotropy increase in vesicles containing gangliosides at both pH 6 and pH 7 ($p < 0.05$). Error bars represent ±1 standard deviation.

Table 3: Effect of Aggregation, pH, and Membrane Composition on Aβ-Induced Changes in DPH Anisotropy[a]

	type 1		type 2	
	pH 7	pH 6	pH 7	pH 6
freshly prepared	0.0 ± 0.1	0.6 ± 0.2	−0.1 ± 0.0	0.0 ± 0.0
2 days aged	1.4 ± 0.1	1.9 ± 0.1	2.0 ± 0.1	2.9 ± 0.2

[a] Aβ (0.5 mg/mL) was aggregated in PBS for the indicated length of time and then diluted into solutions of mixed-composition liposomes containing embedded DPH. Type 1 and type 2 vesicles consist of POPC/POPE/POPS/Chol (36:36:10:18) and POPC/POPE/POPS/Chol/gangliosides (33:33:10:16:8) by mass percent, respectively. Data were analyzed as described in Table 2.

ANS fluorescence at 7 days was considerably diminished relative to 2 days.

Aβ-Induced Changes in Membrane Fluidity of Multicomponent Liposomes. Next, we explored the effect of Aβ on DPH anisotropy in multicomponent liposomes that more closely mimic biological membranes. Results were qualitatively similar to those obtained with single-component liposomes (Figure 9 and Table 3). Without any added Aβ, DPH anisotropy was ∼0.22 in type 1 (POPC/POPE/POPS/Chol) liposomes. The greater anisotropy in type 1 liposomes as compared to POPC or POPG is expected since cholesterol decreases fluidity in membranes above their gel phase transition temperature. Aβ aged for 2 days at pH 7 caused a concentration-dependent increase in DPH anisotropy, but freshly prepared Aβ at pH 7 had no effect (Figure 9a). Freshly prepared Aβ at pH 6 had a marginal effect on DPH anisotropy in type 1 vesicles. Aβ aggregated at pH 6 for 2 days increased DPH anisotropy to a greater extent than did Aβ aggregated at pH 7. The slopes of the anisotropy data vs concentration are substantially smaller for type 1 vs single-phospholipid liposomes (compare Tables 3 and 2). This is likely a consequence of the higher initial anisotropy of the multicomponent liposomes.

Multicomponent liposomes containing 8 wt % gangliosides (type 2 liposomes) were prepared and assessed in the DPH anisotropy assay (Figure 9b and Table 3). Without any added Aβ, DPH anisotropy was ∼0.23 in type 2 liposomes. Freshly prepared Aβ at pH 6 or 7 had no effect on DPH anisotropy. Aβ aggregated for 2 days at pH 6 and pH 7 increased DPH anisotropy in a dose-dependent manner. For both pH 6 and pH 7 aggregates, the anisotropy increase was ∼50% greater with gangliosides present ($p < 0.05$).

Aβ reportedly induces lipid peroxidation under some conditions (*53*, *54*). To explore the possibility that lipid peroxidation caused membrane fluidity changes, we incubated aggregated Aβ with liposomes and tested for the presence of lipid peroxides. In POPC, POPG, type 1, or type 2 vesicles, no significant peroxidation was observed. To further confirm this result, we tested the ability of Aβ aggregates to cause increases in DPH anisotropy in the presence of the antioxidant *n*-propyl gallate (n-PG), which has been reported to reduce Aβ toxicity in cell culture (*55*, *56*). No effect of n-PG was observed (data not shown). Together these data indicate that the Aβ-induced increases in DPH anisotropy are unrelated to any oxidative reactions.

DISCUSSION

Given the amphiphilic nature of Aβ, the location of its C-terminus in the membrane-spanning domain of the precursor protein APP, plus evidence that dissimilar peptides forming structurally similar fibrillar aggregates elicit similar biological responses, it is a plausible hypothesis that Aβ triggers adverse effects on cellular function through interactions with cell membranes. A striking feature of Aβ toxicity is the requirement that the peptide undergo an aggregation process (*1*, *3*). Thus, any Aβ−cell interaction relevant to toxicity must account for this dependence. A key goal in this work was to determine whether changes in membrane physical properties were correlated with Aβ aggregation. Since γ-secretase cleavage of APP at the C-terminus of Aβ may occur in the acidic endosomal-lysosomal system (*4*) and there are drastic morphological and kinetic differences between aggregates prepared at acidic versus neutral pH (*57*, *58*), we also investigated the effect of pH on Aβ aggregation and Aβ-induced changes in membrane properties. Large unilamellar vesicles were chosen as model membrane systems, to provide uniformity in physical properties and control over membrane composition. Membrane fluidity and permeability studies carried out using well-defined liposomes have proven to reliably reflect natural membrane behavior (*59*).

We chose to monitor membrane fluidity as a means to evaluate whether Aβ adversely affects membrane properties in a biologically relevant manner. Proper functioning of integral membrane proteins and signal transduction pathways are sensitive to the local bilayer environment. For example, decreased membrane fluidity disrupts the CCK receptor−G protein complex in rat cortical membranes (*60*) and alters

Na^+/K^+-ATPase activity (*61*). The latter observation is of particular interest to this work in light of reports that Aβ reduces Na^+/K^+-ATPase activity (*62*). Changes in membrane physical properties have been associated with AD in a few reports; in particular, Mecocci et al. (*63*) observed significant decreases in AD mitochondrial membrane fluidity as compared to age-matched controls.

A combination of methodologies were employed to characterize size and surface hydrophobicity of Aβ aggregates as a function of time and pH. Insoluble aggregates were formed essentially instantaneously upon dilution of monomeric Aβ into acidic pH buffer, with roughly 80−85% of peptide in an aggregated form. These aggregates bound to bis-ANS strongly, indicating the presence of hydrophobic patches commonly observed in partially folded or misfolded proteins. In contrast, dilution of monomeric Aβ into neutral pH buffer led to the formation of soluble (optically clear) aggregates. Only 25−35 wt % of Aβ at pH 7 was aggregated into high molecular mass (>100 kDa) species. These fibrillar aggregates grew slowly and continually over 4 days. After 4 days of aggregation, the rate of growth increased and the morphology shifted to a slightly branched or entangled structure followed by the appearance of insoluble macroscopic aggregates. Freshly diluted Aβ at pH 7 did not bind bis-ANS. Soluble aggregates during the growth phase contained hydrophobic patches that bound bis-ANS, but these were lost after formation of a precipitate phase (~7 days).

We propose the following interpretation of these data. Freshly diluted Aβ is monomeric and does not display a sufficiently large hydrophobic area to bind bis-ANS. Dilution of monomeric Aβ into PBS at neutral pH initiates rapid folding and orderly association into fibrils, driven by a balance of hydrophobic collapse and electrostatic interactions. Hydrophobic patches are generated as Aβ folds and associates into fibrils. The predominant growth mechanism is via fibril elongation, as evidenced by the nearly constant ratio of molecular weight to fibril length (Figure 3). As fibrils become sufficiently long (~4 days), fibril−fibril contact occurs, leading to near-complete burial of hydrophobic surfaces (evidenced by loss of bis-ANS fluorescence), fibril−fibril entanglement (detected by static light scattering), and eventual formation of a second phase.

At pH 6, Aβ is near its p*I* of 5.5 (*58*) and is susceptible to isoelectric precipitation. A greater fraction of the peptide is converted to aggregates, as evidenced by the size-exclusion results; the surface of the aggregates is hydrophobic and binds bis-ANS, and the gross aggregate morphology is nonfibrillar (Figure 4b). Consistent with these results, Wood et al. (*58*) observed a greater fraction of amorphous, nonfibrillar aggregates with Aβ aggregated at pH 5.8, and Walsh et al. (*64*) reported that Aβ at pH 6 formed a "mat" of filamentous aggregates that were distinctly different than fibrils formed at pH 7. The rapid association of Aβ at pH 6 appears to generate large quantities of partially folded aggregates that agglomerate into an insoluble structure.

An understanding of the physical structure of Aβ aggregates is useful for interpreting the DPH anisotropy results. We observed that aggregated, but not monomeric, Aβ at pH 7 induced decreases in membrane fluidity in all four types of liposome preparations investigated. The increase in potency over the first 2 days of aggregation correlated with the continued growth of aggregates over the same period. The potency of Aβ decreased slightly at 4 days and essentially disappeared after 7 days of aggregation. These changes can be related to changes in Aβ aggregate structure: after 4 days there was an increase in the growth rate observed by dynamic light scattering and a change in morphology observed by static light scattering. At 7 days, there was formation of a precipitate phase and a loss of bis-ANS binding. We propose that self-association of monomeric Aβ into soluble fibrils generates hydrophobic patches at the fibril surface that facilitate interaction of Aβ aggregates with the acyl chains of the bilayer core, restricting chain mobility. These hydrophobic patches also drive fibril−fibril assembly, leading to eventual burial of the hydrophobic areas. There is a subsequent loss of membrane activity after surface hydrophobicity is buried. It is interesting to speculate whether the loss of membrane activity after 7 days is related to the "overaging" effect reported by some, in which Aβ loses some of its toxic potency in cell culture assays (*65*).

Both fresh and aggregated Aβ at pH 6 induced decreases in membrane fluidity. These decreases were ~50−100% greater for pH 6 than for pH 7 aggregates at 2−3 days of aging time. Concordantly, Aβ monomer diluted into pH 6 buffer aggregated immediately, and bis-ANS fluorescence intensity for pH 6 aggregates was roughly twice that for pH 7 aggregates. Unlike pH 7 aggregates, neither bis-ANS fluorescence nor DPH anisotropy was attenuated with longer aggregation time. These results also provide additional support for the hypothesis that hydrophobic patches on the surface of partially folded Aβ aggregates are responsible for membrane interactions.

Since DPH is buried deep within the acyl chain region of the bilayer, increases in anisotropy report on decreased acyl chain mobility and increased chain order in the hydrophobic core (*35*, *36*). Such changes are typically observed with insertion of hydrophobic peptides into a membrane (*66*). For example, functional mutant OmpA signal peptides possess high hydrophobic content, insert into membranes, and increase DPH anisotropy (*67*). Similarly, a peptide fragment from the cytotoxic protein α-sarcin penetrates into the hydrophobic core of the bilayer and substantially increases DPH anisotropy at temperatures above the phase transition (*68*). These peptides share many similarities with Aβ: β-strand fold, a fairly high hydrophobic content, and for OmpA peptides, a propensity to aggregate. We propose therefore that Aβ aggregates induce decreases in membrane fluidity via bilayer penetration.

The similarity in response of both POPC and POPG liposomes suggests that the effect is not strongly dependent on the nature of the polar headgroup and that changes in membrane fluidity are not simply the result of electrostatic binding of Aβ to the bilayer surface. At pH 7, but not at pH 6, there were small but statistically significant differences in the effect of Aβ on POPC vs POPG liposomes at all time points (Table 2), with the former being less sensitive. POPC and POPG share identical acyl tails and a common melting temperature (−2 °C). One possible explanation is that the difference is caused by POPG-catalyzed conversion of monomeric Aβ from random coil to β-sheet and induction of Aβ aggregation (*13*−*15*). POPC and other phospholipids with zwitterionic headgroups do not catalyze these changes (*15*). At pH 6, conversion to β-sheet aggregates is already

heavily favored (*69*, *70*), thus any catalytic activity is redundant.

For POPC and POPG vesicles, the magnitude of the change in membrane fluidity observed was quite significant: DPH anisotropy increased from a value of $r \sim 0.14$, indicative of a highly mobile fluid phase, to $r > 0.3$, comparable to a gellike bilayer. Aggregated Aβ also decreased membrane fluidity of more biologically realistic mixed liposomes, although the magnitude of the effect was smaller. This is likely due simply to the higher initial anisotropy (no added Aβ) with the mixed liposomes, since the maximum observable DPH anisotropy in membranes is 0.3−0.34 (*35*). This result predicts that aggregated Aβ would generally have a larger effect on more fluid membranes.

The addition of gangliosides in type 2 liposomes enhanced Aβ-mediated changes in membrane fluidity at both pH 6 and 7 (Figure 9b and Table 3) but only when Aβ was aggregated. Binding of Aβ to gangliosides embedded in membranes has been widely described (*16*, *17*, *21*, *71)* although the results of these interactions have been variably reported as acceleration of Aβ aggregation (*16*), inhibition of Aβ aggregation and stabilization of an α-helical structure (*17*), or induction of a β-sheet structure (*21*). Our results do not address the specific issues of structural changes induced by gangliosides but do support the hypothesis that gangliosides enhance Aβ−membrane interactions.

Our results agree with those obtained by Müller and coworkers (*24*, *25*) and Chauhan et al. (*26*); both groups reported decreases in membrane fluidity, detected as an increase in DPH anisotropy, in PE/PC/cardiolipin small unilamellar vesicles (*26*) or mouse brain or human cortex homogenates (*24*, *25*). Other groups have reported the opposite effect, namely, increases in membrane fluidity in response to Aβ using the fluorescent dye pyrene (*27*, *28*) or other methods (*21*, *28*). Several possible reasons for these discrepancies include differences in response of liposomes and homogenates as compared to synaptic plasma membranes (*28*), differences in aggregation and/or conformational state of Aβ, differences in methods of contacting Aβ with membranes, and differences in the physical location of probe molecules within the bilayer (*25*).

Under our experimental conditions, Aβ did not cause lipid peroxidation, and the antioxidant n-PG was ineffective at preventing decreases in membrane fluidity induced by Aβ aggregates. Recently, Dikalov et al. (*72*) reported that Aβ alone is unable to spontaneously generate free radicals, in contrast to previous reports (*54*). Taken together, our data indicate that Aβ-induced decreases in membrane fluidity are independent of oxidative reactions and result from physical contact between hydrophobic regions of Aβ aggregates and the hydrophobic core of the lipid bilayer.

ACKNOWLEDGMENT

The authors acknowledge stimulating discussions with Dr. Jyothi Ghanta in the initiation of this project. Randall Massey in the UW Medical School Electron Microscopy Facility contributed the electron micrographs. Dr. Ron Raines provided access to a spectrofluorometer for part of this project.

REFERENCES

1. Pike, C. J., Burdick, D., Walencewicz, A. J., Glabe, C. G., and Cotman., C. W. (1993) *J. Neurosci. 13*, 1676−1687.
2. Simmons, L. K., May, P. C., Tomaselli, K. J., Rydel, R. E., Fuson, K. S., Brigham, E. F., Wright, S., Lieberburg, I., Becker, G. W., Brems, D. N., and Li, W. (1994) *Mol. Pharmacol. 45*, 373−379.
3. Iverson, L. L., Mortishire-Smith, R. J., Pollack, S. J., and Shearman, M. S. (1995) *Biochem. J. 311*, 1−16.
4. Mattson, M. P. (1997) *Physiol. Rev. 77*, 1081−1132.
5. Joslin, G., Krause, J. E., Hershey, A. D., Adams, S. P., Fallon, R. J., and Perlmutter, D. H. (1991) *J. Biol. Chem. 266*, 21897−21902.
6. El Khoury, J., Hickman, S. E., Thomas, C. A., Cao, L., Silverstein, S. C., and Loike, J. D. (1996) *Nature 382*, 716−719.
7. Yan, S. D., Chen, X., Fu, J., Chen, M., Zhu, H., Roher, A., Slattery, T., Zhao, L., Nagashima, M., Morser, J., Migheli, A., Nawroth, P., Stern, D., and Schmidt, A. M. (1996) *Nature 382*, 685−691.
8. Yan, S. D., Fu, J., Soto, C., Chen, X., Zhu, H., Al-Mohanna, F., Collison, K., Zhu, A., Stern, E., Saido, T., Tohyamas, M., Ogawa, S., Roher, A., and Stern, D. (1997) *Nature 389*, 689−695.
9. Schultz, J. G., Megow, D., Reszka, R., Villringer, A., Einhaupl, K. M., and Dimagi, U. (1998) *Eur. J. Neurosci. 10*, 2085−2093.
10. Cribbs, D. H., Pike, C. J., Weinstein, S. L., Velazquez, P., and Cotman, C. W. (1997) *J. Biol. Chem. 272*, 7431−7436.
11. Tucker, H. M., Rydel, R. E., Wright, S., and Estus, S. (1998) *J. Neurochem. 71*, 506−516.
12. Good, T., and Murphy, R. M. (1995) *Biochem. Biophys. Res. Commun. 207*, 209−215.
13. Seelig, J., Lehrmann, R., and Terzi, E. (1995) *Mol. Membr. Biol. 12*, 51−57.
14. Terzi, E., Hölzemann, G., and Seelig, J. (1995) *J. Mol. Biol. 252*, 633−642.
15. Terzi, E., Hölzemann, G., and Seelig, J. (1997) *Biochemistry 36*, 14845−14852.
16. Choo-Smith, L.-P., and Surewicz, W. K. (1997) *FEBS Lett. 402*, 95−98.
17. McLaurin, J., Franklin, T., Fraser, P. E., and Chakrabarrty, A. (1998) *J. Biol. Chem. 273*, 4506−4515.
18. Arispe, N., Pollard, H. B., and Rojas, E. (1993) *Proc. Natl. Acad. Sci. U.S.A. 90*, 10573−10577.
19. McLaurin, J., and Chakrabartty, A. (1996) *J. Biol. Chem. 271*, 26482−26489.
20. Pillot, T., Goethals, M., Vanloo, B., Talussot, C., Brasseur, R., Vanderkerckhove, J., Rosseneu, M., and Lins, L. (1996) *J. Biol. Chem. 271*, 28757−28765.
21. Matsuzaki, K., and Horikiri, C. (1999) *Biochemistry 38*, 4137−4142.
22. Yang, A. J., Chandswangbhuvana, D., Margol, L., and Glabe, C. G. (1998) *J. Neurosci. Res. 52*, 691−698.
23. Hertel, C., Terzi, E., Hauser, N., Jakob-Røtne, R., Seelig, J., and Kemp, J. A. (1997) *Proc. Natl. Acad. Sci. U.S.A. 94*, 9412−9416.
24. Müller, W. E., Koch, S., Eckert, A., Hartmann, H., and Scheuer, K. (1995) *Brain Res. 674*, 133−136.
25. Müller, W. E., Eckert, G. P., Scheuer, K., Cairns, N. J., Maras, A., and Gattaz, W. F. (1998) *Amyloid 5*, 10−15.
26. Chauhan, A., Chauhan, V. P. S., Brockerhoff, H., and Wisniewski, H. M. (1993) *Alzheimer's Disease: Advances in Clinical and Basic Research*, pp 431−439, John Wiley & Sons Ltd, New York.
27. Avdulov, N. A., Chochina, S. V., Igbavboa, U., O'Hare, E. O., Schroeder, F., Cleary, J. P., and Wood, W. G. (1997) *J. Neurochem. 68*, 2086−2091.
28. Mason, R. P., Jacob, R. F., Walter, M. F., Mason, P. E., Avdulov, N. A., Chochina, S. V., Igbavboa, U., and Wood, W. G. (1999) *J. Biol. Chem. 26*, 18801−18807.
29. Bretscher, M. (1973) *Science 181*, 622−629.
30. Söderberg, M., Edlund, C., Kristensson, K., and Dallner, G. (1990) *J. Neurochem. 54*, 415−423.

31. Svennerholm, L., Boström, K., Jungbjer, B., and Olsson, L. (1994) *J. Neurochem. 63*, 1802−1811.
32. Demetrio, R. S., Antunesmadeira, M. D., and Madeira, V. M. C. (1998) *Med. Sci. Res. 26*, 557−561.
33. Van Ginkel, G., Van Langen, H., and Levine, Y. K. (1989) *Biochimie 71*, 23−32.
34. Schroeder, F. (1988) *Methods for Studying Membrane Fluidity. Advances in Membrane Fluidity*, Vol. 1, pp 193-219, Alan R. Liss Inc., New York.
35. Lentz, B. R. (1989) *Chem. Phys. Lipids 50*, 171−190.
36. Lentz, B. R. (1993) *Chem. Phys. Lipids 64*, 117−127.
37. Mills, J., and Reiner, P. B. (1999) *J. Neurochem. 72*, 443−460.
38. Shen, C.-L., and Murphy, R. M. (1995) *Biophys. J. 69*, 640−651.
39. Snyder, S. W., Ladror, U. S., Wade, W. S., Wang, G. T., Barrett, L. W., Matayoshi, E. D., Huffaker, H. J., Krafft, G. A., and Holzman, T. F. (1994) *Biophys. J. 67*, 1216−1228.
40. Shen, C.-L., Fitzgerald, M. C., and Murphy, R. M. (1994) *Biophys. J. 65*, 2383−2395.
41. Pallitto, M. M., Ghanta, J., Heinzelman, P., Kiessling, L. L., and Murphy, R. M. (1999) *Biochem. 38*, 3570−3578.
42. Stewart, W. E., and Sorensen, J. P. (1981) *Technometrics 23*, 131−141.
43. Stryer, L. (1965) *J. Mol. Biol. 13*, 482−495.
44. Turner, D. C., and Brand, L. (1968) *Biochemistry 7*, 3381−3390.
45. Lakowicz, Joseph R. (1986) *Principles of Fluorescence Spectrocopy*; Plenum Press, New York.
46. Walter, M. F., Mason, P. E., and Mason, R. P. (1997) *Biochem. Biophys. Res. Commun. 233*, 760−764.
47. El-Saadani, M., Esterbauer, H., El-Sayed, M., Goher, M., Nassar, A. Y., and Jürgens, G. (1989) *J. Lipid Res. 30*, 627−630.
48. Tirado, M. M., Martinez, C. L., and Garcia de la Torre, J. (1984) *J. Chem. Phys. 81*, 2047−2052.
49. Levine, H., III (1993) *Protein Sci. 2*, 404−410.
50. Gibbons, D. L., and Horowitz, P. M. (1995) *J. Biol. Chem. 270*, 7335−7340.
51. Sudhakar, K., and Fay, P. J. (1996) *J. Biol. Chem. 271*, 23015−23021.
52. Mitchell, D. C., and Litman, B. J. (1998) *Biophys. J. 75*, 896−908.
53. Behl, C., Davis, J. B., Lesley, R., and Schubert, D. (1994) *Cell 77*, 817−827.
54. Butterfield, D. A., Hensley, K., Harris, M., Mattson, M. and Carney, J. (1994). *Biochem. Biophys. Res. Commun. 200*, 710−715.
55. Behl, C., Davis, J., Cole, G. M., and Schubert, D. (1992) *Biochem. Biophys. Res. Commun. 186*, 944−950.
56. Mattson, M. P., and Goodman, Y. (1995) *Brain Res. 676*, 219−224.
57. Burdick, D., Soreghan, B., Kwon, M., Kosmoski, J., Knauer, M., Henschen, A., Yates, J., Cotman, C., and Glabe, C. (1992) *J. Biol. Chem. 267*, 546−554.
58. Wood, S. J., Maleeff, B., Hart, T., and Wetzel, R. (1996) *J. Mol. Biol. 256*, 870−877.
59. Magin, R. L., Niesman, M. R., and Bacic, G. (1990) *Adv. Membr. Fluid. 4*, 221−237.
60. Rinken, A., Harro, J., Engström, L., and Oreland, L. (1998) *Biochem. Pharmacol. 55*, 423−431.
61. Deliconstantinos, G. (1985) *Neurochem. Res. 10*, 1605−1613.
62. Mark, R. J., Hensley, K., Butterfield, D. A., and Mattson, M. P. (1995) *J. Neurosci. 15*, 6239−6249.
63. Mecocci, P., Beal, M. F., Cecchetti, R., Polidori, M. C., Cherubini, A., Chionne, F., Avellini, L., Romano, G., and Senin, U. (1997) *Mol. Chem. Neuropath. 31*, 53−64.
64. Walsh, D. M., Hartley, D. M., Kusumoto, Y., Fezoui, Y., Condron, M. M., Lomakin, A., Benedek, G. B., Selkoe, D. J., and Teplow, D. B. (1999) *J. Biol. Chem. 274*, 25945−25952.
65. Mattson, M. P., Furukawa, K., Bruce, A. J., Mark, R. J., and Blanc, E. M. (1996) *Molecular Mechanisms of Dementia*; Humana, Totowa, NJ, 103−143.
66. Papahadjopoulos, D., Moscarello, M., Eylar, E. H., and Isac, T. (1975) *Biochim. Biophys. Acta 401*, 317−345.
67. Hoyt D. W., and Gierasch, L. M. (1991) *Biochemistry 30*, 10155−10163.
68. Mancheno, J. M., Gasset, M., Albar, J. P., Lacadena, J., Martinez del Pozo, A., Onaderra, M., and Gavilanes, J. G. (1995) *Biophys. J. 68*, 2387−2395.
69. Barrow, C. J., and Zagorski, M. G. (1991) *Science 253*, 179−182.
70. Barrow, C. J., Yasuda, A., Kenny, P. T., and Zagorski, M. G. (1992) *J. Mol. Biol. 225*, 1075−1093.
71. Yanagisawa, K., and Ihara, Y. (1998) *Neurobiol. Aging 19*, S65−67.
72. Dikalov, S. I., Vitek, M. P., Maples, K. R., and Mason, R. P. (1999) *J. Biol. Chem. 274*, 9392−9399.

BI0001980